

LETTER

Open Access



# Localized field-aligned currents and 4-min TEC and ground magnetic oscillations during the 2015 eruption of Chile's Calbuco volcano

Tadashi Aoyama<sup>1\*</sup>, Toshihiko Iyemori<sup>1</sup>, Kunihiro Nakanishi<sup>1</sup>, Michi Nishioka<sup>2</sup>, Domingo Rosales<sup>3</sup>, Oscar Veliz<sup>3</sup> and Erick Vidal Safor<sup>3</sup>

## Abstract

The Calbuco volcano in southern Chile erupted on April 22, 2015. About 2 h after the first eruption, a Swarm satellite passed above the volcano and observed enhancement of small-amplitude (~0.5 nT) magnetic fluctuations with wave-packet structure which extends 15° in latitude. Similar wave packet is seen at the geomagnetic conjugate point of the volcano. Just after the eruption, geomagnetic fluctuations with the spectral peaks around the vertical acoustic resonance periods, 215 and 260 s, were also observed at Huancayo Geomagnetic Observatory located on the magnetic equator. Besides these observations, around 4-min, i.e., 175, 205 and 260 s, oscillations of total electron content (TEC) were observed at global positioning system stations near the volcano. The horizontal propagation velocity and the spatial scale of the TEC oscillation are estimated to be 720 m/s and 1600 km, respectively. These observations strongly suggest that the atmospheric waves induced by explosive volcanic eruption generate TEC variation and electric currents. The Swarm observation may be explained as a manifestation of their magnetic effects observed in the topside ionosphere.

**Keywords:** Magnetic field, Magnetic fluctuation, Field-aligned current, Acoustic gravity wave, Middle latitudes, Atmospheric wave, Ionospheric dynamo, Volcanic eruption, Total electron content, Ionospheric disturbance

## Introduction

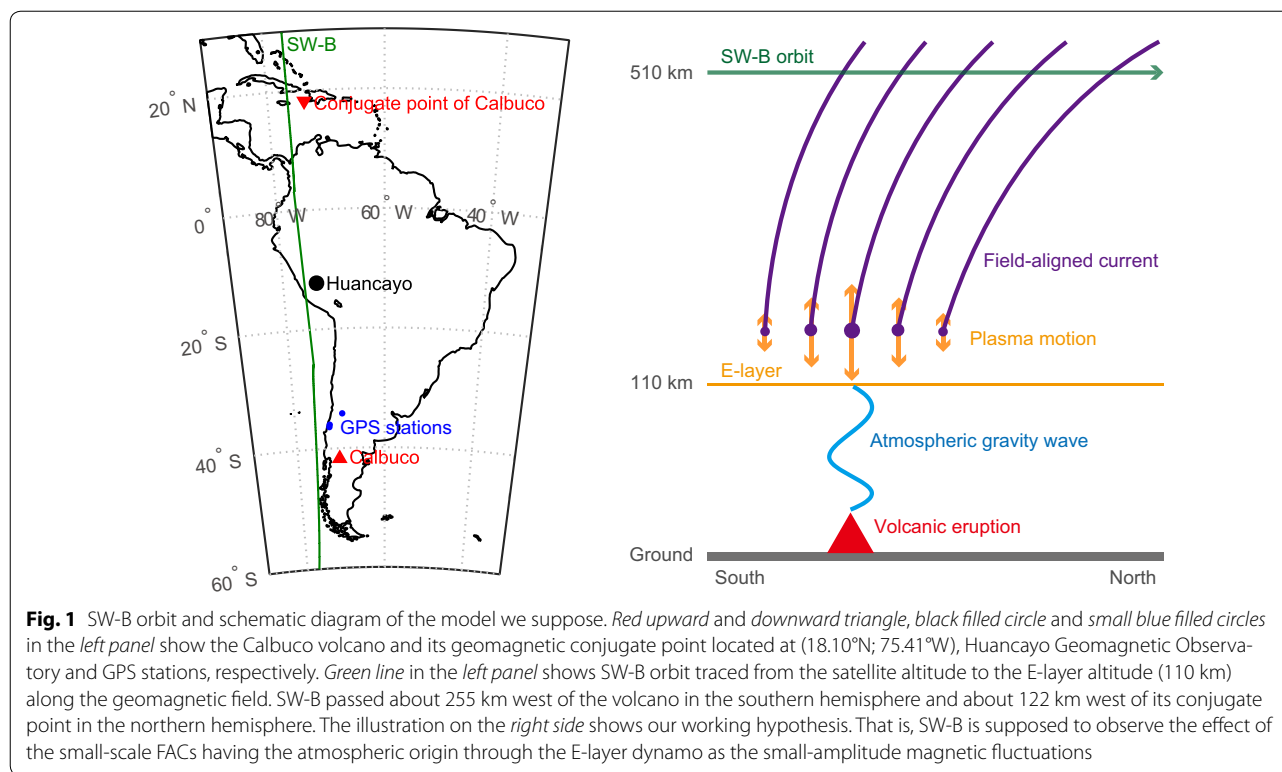
The low earth orbit satellite, CHAMP, equipped with precise magnetometers was launched in 2000. Nakanishi et al. (2014) found in the CHAMP magnetic data that small-amplitude (1–5 nT on the dayside) magnetic fluctuations with periods of a few tens of seconds (20–40 s) along the satellite orbit were almost always observed in middle and low latitudes in the topside ionosphere (see Nakanishi et al. 2014, Figure 2). We name these magnetic fluctuations “magnetic ripples” (MRs). They interpreted the MRs as the magnetic effects of small-scale field-aligned currents (FACs) generated through the ionospheric dynamo process induced by the waves from lower

atmosphere. Their model is, (1) atmospheric disturbance induces gravity waves including acoustic mode waves, and they propagate upward, (2) neutral wind accompanied by the waves drives dynamo electric current in the ionospheric E-layer within limited area where the waves are injected, (3) divergent perpendicular dynamo currents give rise to FACs, and (4) low-altitude satellite observes the spatial structure of the FACs as the temporal magnetic fluctuations along the orbit. The schematic diagram in Fig. 1 (right panel) shows the model we suppose in this study.

The Swarm constellation was launched on November 22, 2013, into a near-polar orbit. Iyemori et al. (2015) confirmed that the MRs observed by Swarm satellites on the initial orbits are spatial structure of FACs. Time-scale of their temporal variations is roughly estimated to

\*Correspondence: aoyama@kugi.kyoto-u.ac.jp

<sup>1</sup> Graduate School of Science, Kyoto University, Kyoto, Japan  
Full list of author information is available at the end of the article



be 200–340 s, and amplitudes of the MRs shown in their paper are about 1 nT. The typical latitudinal scale of the MRs is estimated to be 100 km in Nakanishi et al. (2014).

Above two papers suggest that the origin of the MRs observed by CHAMP and Swarm is most likely to be the acoustic gravity waves (AGWs) from lower atmosphere. However, the evidence reported so far is not sufficient enough to account for lower atmospheric origin. The aim of this study is to add a supporting evidence on the origin of the MRs by analyzing a case of volcanic eruption which is known to generate atmospheric gravity waves. For example, Kanamori and Mori (1992) reported for the first time that the acoustic coupling of the atmosphere and the solid Earth induced the long-period Rayleigh waves having a vertical acoustic resonance (VAR) period of 270 s, associated with the 1991 eruption of Mt. Pinatubo. The merit of analyzing volcanic eruption events is that a volcanic eruption is a point source of the atmospheric gravity waves with known onset time. On the other hand, severe meteorological phenomena such as tropical cyclones which are known to generate the gravity waves (e.g., Sato 1993; Suzuki et al. 2013) have widely extended region so that it is not easy to identify the source location of the MRs.

It has been observed that natural phenomena on the Earth's surface or in the troposphere affect the

ionosphere. After volcanic eruption (e.g., Heki 2006; Dautermann et al. 2009) or massive tornado (e.g., Nishioka et al. 2013), disturbances in total electron content (TEC) have been observed. After great earthquakes, short-period magnetic and atmospheric pressure oscillations (e.g., Iyemori et al. 2005, 2013) or TEC variations (e.g., Otsuka et al. 2006; Saito et al. 2011) were observed. As to the theoretical study, TEC oscillations observed after the 2011 off the Pacific coast of Tohoku Earthquake and FACs in the ionosphere generated by acoustic mode waves were well reproduced with numerical simulations by Matsumura et al. (2011) and by Zettergren and Snively (2013), respectively. Zettergren and Snively (2015) performed the computer simulations showing that TEC and ground-level magnetic field perturbations and dynamo FACs can be caused by natural hazard events including volcanic eruptions.

In this study, we report a set of observations which supports the above model of a MR generation mechanism. That is, (1) small-scale FACs, (2) spectral peaks at the VAR in geomagnetic field and (3) TEC oscillations caused by the AGWs generated during the 2015 eruption of Chile's Calbuco volcano were observed by a Swarm satellite, the ground magnetometer at Huancayo, and global positioning system (GPS) receivers around the volcano, respectively.

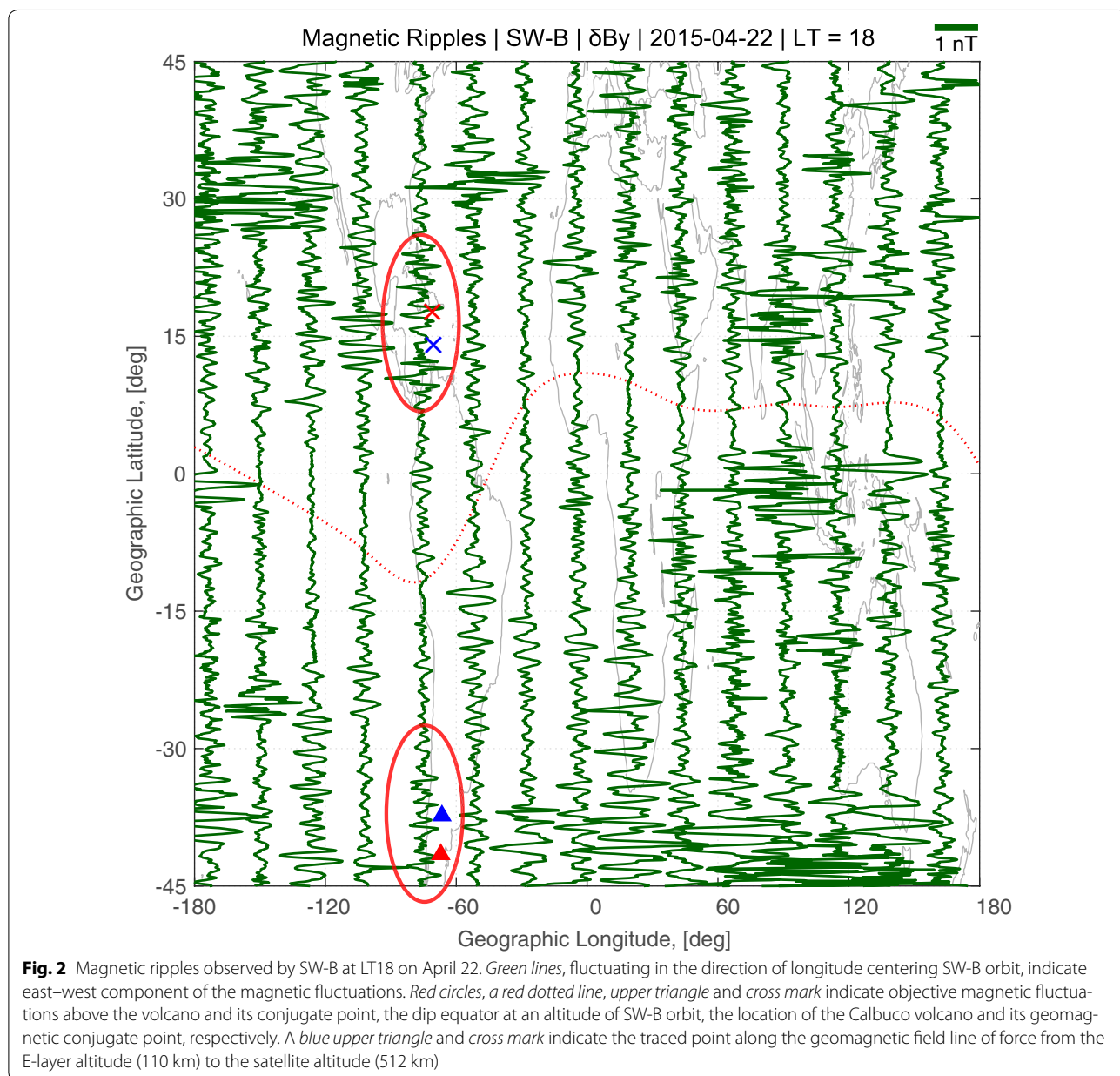
**Observations**

The Calbuco volcano located at (41.33°S; 72.62°W), one of the most active volcanoes in Chile, erupted on April 22, 2015. The first eruption occurred at around 21:08 UTC and lasted about 90 min. By a Swarm satellite, a ground magnetic observatory, and GPS stations, we observed electromagnetic phenomena possibly induced by the volcanic eruption.

**Satellite observation**

The Swarm constellation consists of three satellites (SW-A, SW-B and SW-C). After April 17, 2014, SW-A and

SW-C fly side by side at an altitude of about 460 km, while SW-B flies at about 50 km higher altitude than those of SW-A and SW-C. Their velocity and orbital period are about 7.5 km/s and 90 min, respectively. The vector field magnetometer on board the Swarm satellites has a resolution of 0.0625 nT which is sufficient to identify the MRs (0.1–5 nT). As illustrated on the map and the schematic diagram in Fig. 1, SW-B passed about 255 km west and 510 km altitude above the volcano from south to north about 2 h after the first eruption, and SW-A and SW-C passed about 600 km west of the volcano about 30 min after the eruption. In this study, we use only SW-B



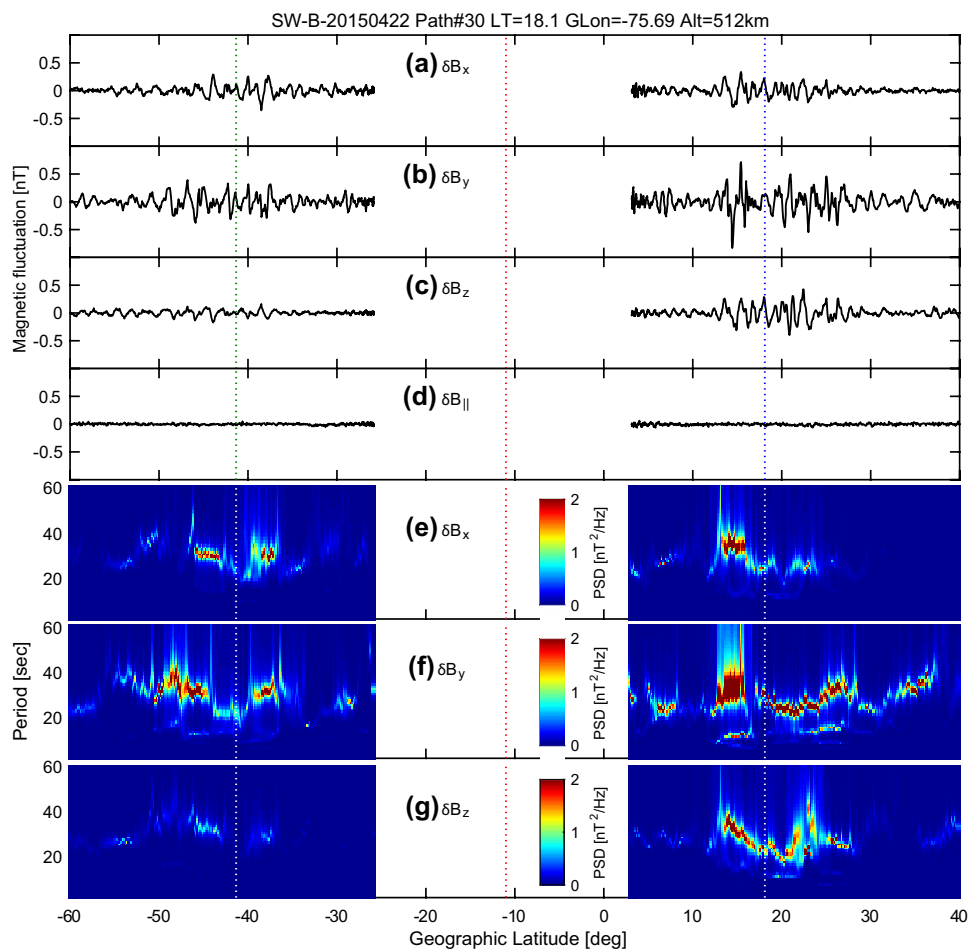


**Fig. 3** Magnetic ripples observed by SW-B 2 h after the eruption. **a** The vertical component, **b** the east–west component and **c** the north–south component in the sensor coordinate system. **d** The parallel component to the geomagnetic main field. *Orange, blue and green dotted lines* indicate the latitudes of Calbuco volcano, its geomagnetic conjugate point and the dip equator, respectively. **e–g** Dynamic spectra of magnetic field (**a–c**) along the satellite path. The *horizontal and vertical axes* indicate the geographic latitude of the footprint at 110 km altitude traced from satellite position along the geomagnetic field and period, respectively. *Color* indicates power spectral density

one-second average data because the orbits of SW-A and SW-C were rather far from the volcano.

Figure 2 shows the east–west component of the magnetic fluctuations observed by SW-B on April 22, 2015. There exist many MRs with similar amplitude; however, the characteristics shown in the following section suggest that the observed MR over the volcano and its magnetic conjugate point may be related to the volcanic eruption. We should note that the large amplitude fluctuations near the bottom edge of the figure are not the MRs but probably the effects from polar electromagnetic phenomena.

Figure 3a–d shows the fluctuations of magnetic fields in the sensor coordinate system ( $X$ ,  $Y$  and  $Z$ ) and that of the parallel component to the geomagnetic main field observed by SW-B above the volcano about 2 h after the eruption. The  $X$ ,  $Y$  and  $Z$  indicate the vertical, east–west

and north–south directions, respectively. The horizontal axis is the geographic latitude traced from the satellite (at altitude  $\sim 510$  km) to the dynamo layer (at altitude 110 km) along the magnetic field calculated with International Geomagnetic Reference Field 12th generation (Thébault et al. 2015). The vertical axis is the magnetic fluctuation obtained from high-pass filtering with a cut-off period about 40 s in order to remove the geomagnetic main field and other longer spatial scale phenomena than the MRs including the effect of equatorial electrojet. Figure 3e–g shows the dynamic spectra of the magnetic fluctuations along the satellite path. The horizontal axis is same as Fig. 3a–c. The vertical axis and color scale show period and power spectral density (PSD), respectively. Because the geomagnetic lines of force do not reach satellite altitudes near the dip equator ( $-23^\circ$  to  $3^\circ$

in geographic latitude), there appears a gap in the latitude range  $0^\circ$  to  $\pm 13^\circ$  from the dip equator.

Following features are shown in Fig. 3.

1. Amplitudes of the MRs enhance at the latitudes over the volcano and also at geomagnetic conjugate point.
2. The amplitude enhancements show packet-like structure, and those in the northern hemisphere are larger, where the satellite flew more closely (i.e., 155 km west) to the magnetic conjugate point of the volcano.
3. Maximum amplitude of  $\delta B_y$  (east–west component) is the largest among three components.
4. Parallel component to the observed geomagnetic field ( $\delta B_{\parallel}$ ) is almost zero.
5. The dynamic spectra clearly show a symmetric structure with respect to the dip equator. They also show a roughly symmetric latitudinal distribution with respect to the location of the volcano and its conjugate point.

As shown in Fig. 3a–c, the latitudinal zones of the amplitude enhancement in both hemispheres have packet-like structure having a width of about  $15^\circ$  in latitude (about 1700 km in horizontal distance). Spectral peak of the MRs in the packet-like structure is about 24 s (on average). Therefore, a dominant spatial scale of the FACs is about 180 km derived from 7.5 km/s (horizontal

velocity of SW-B)  $\times$  24 s. The SW-B passed about 255 km west of the volcano in the southern hemisphere, and about 122 km west of the magnetic conjugate point in the northern hemisphere, i.e., the distance between SW-B orbit and the volcano is longer than the distance between SW-B orbit and the conjugate point of the volcano. This may be the reason why the amplitudes in the northern hemisphere are larger than those in the southern hemisphere as shown in Fig. 3. In addition, it should be noted that  $\delta B_{\parallel}$  is almost zero at any latitudes (Fig. 3d). That is, the MRs are generated by the currents parallel to the geomagnetic field, and they are not the effect of plasma bubbles where  $\delta B_{\parallel}$  also fluctuates (Stolle et al. 2006; Park et al. 2009).

### Ground observation

Figure 4d, e, respectively, shows the time series of H (horizontal) and D components (orthogonal to the horizontal component in the horizontal plane and presented in nT unit) of the geomagnetic fluctuations at Huancayo observatory. A band-pass filter of 215–235 s was used in order to remove the effects from other source and to compare with the GPS-TEC variations in Fig. 4a–c. A similar packet structure is seen in the red dotted rectangles in both GPS-TEC and H component of geomagnetic field (Fig. 4c, d). There exists a 608-s time difference between the two rectangles. As discussed in the following

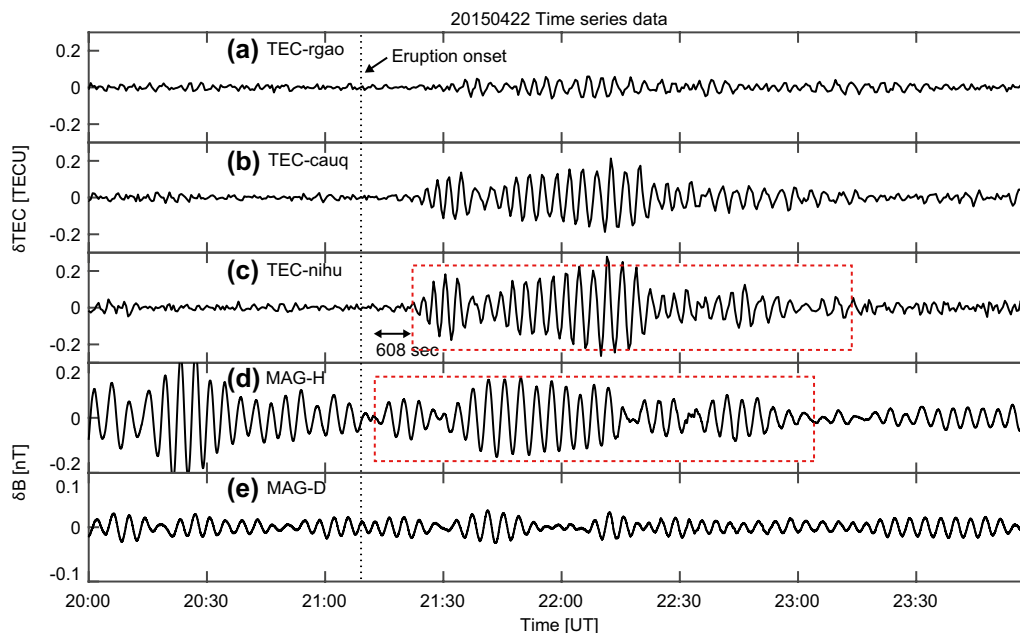
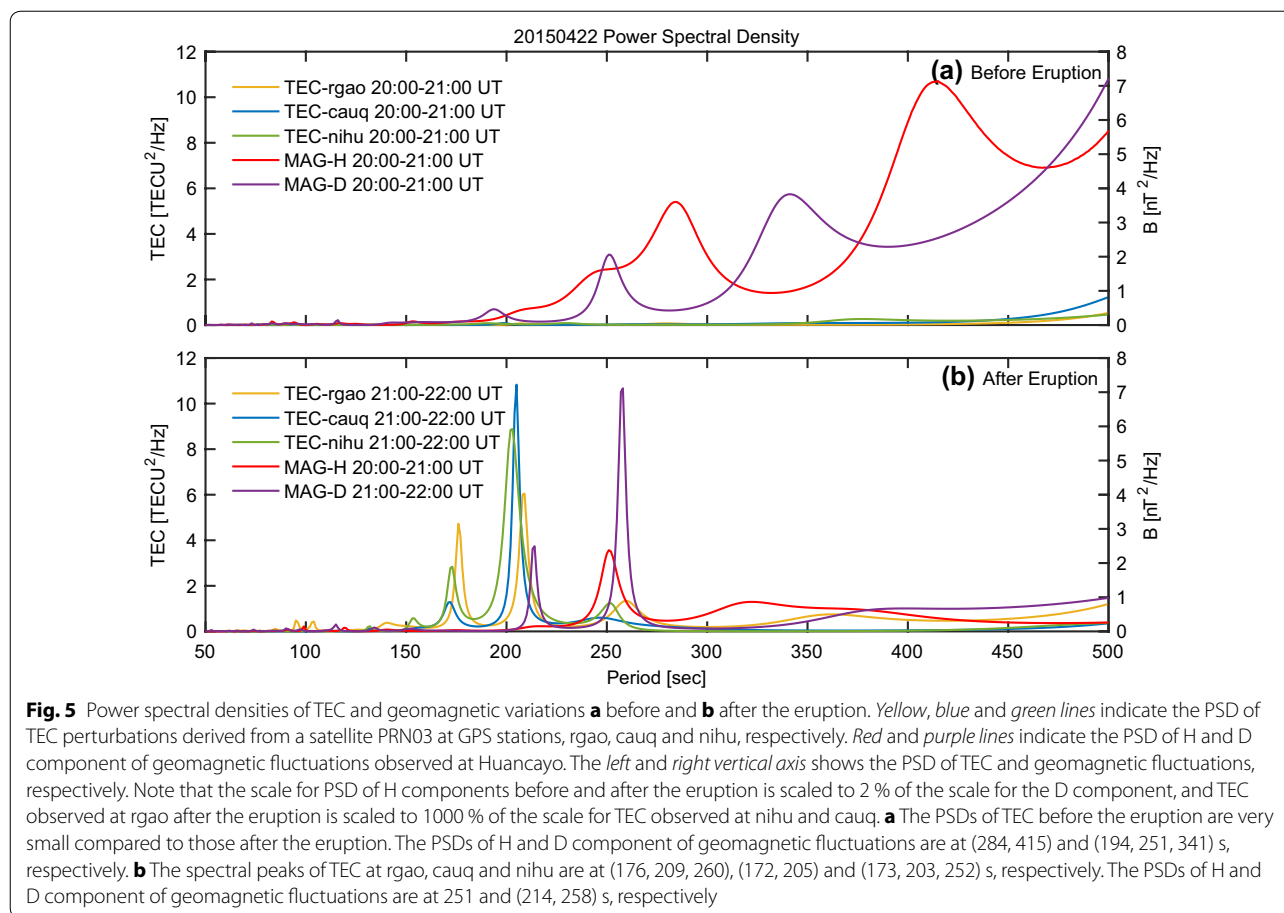


**Fig. 4** Time series of TEC and geomagnetic variations. TEC perturbations derived from a satellite PRN03 at GPS stations, **a** rgao, **b** cauq and **c** nihu. Time series of horizontal (**d**) and declination (**e**) component of geomagnetic field observed at Huancayo observatory. A band-pass filter of 215–235 s was used. Vertical dotted line shows the onset time of the eruption (around 21:08). Similar packet structures are seen in the red dotted rectangles in GPS-TEC and H component of geomagnetic field. There is a 608-s time difference between the two rectangles in **c** and **d**



section, we interpret the geomagnetic fluctuations shown in Fig. 4d, e as the effect of a current system generated by the VAR induced by the volcanic eruption. Red and purple lines in Fig. 5 show the PSDs of H and D components of geomagnetic variation observed at Huancayo before (Fig. 5a) and after (Fig. 5b) the volcanic eruption, respectively. Sharp spectral peaks at 251 s in H component (a red line in Fig. 5b) and at 258 and 214 s in D component (a purple line in Fig. 5b) are seen after the eruption. These periods are close to theoretically predicted periods of the VAR (e.g., Tahira 1995; Nishida et al. 2000; Shinagawa et al. 2007). There are similar spectral peaks, although not very sharp, at 284 s in H component (a red line in Fig. 5a) and 251 and 194 s in D component (a purple line in Fig. 5a) before the eruption; these amplitudes are smaller than those after the eruption although the local time is more close to noon where the ionospheric conductivity, in particular the Cowling conductivity, is higher.

#### TEC observation

We make use of the 30-s averaged TEC data derived from a GPS satellite, PRN03, at three stations near the volcano,

“rgao” located at (34.2°S; 69.4°W), “cauq” at (36.0°S; 72.3°W) and “nihu” at (36.4°S; 72.4°W). Figure 4a–c shows the time series of TEC perturbations at the three GPS stations. The data have been detrended and high-pass-filtered with cutoff period about 10 min. We see clear “4-min oscillations” started at 15–30 min after the eruption. Yellow, blue and green lines in Fig. 5 show the power spectral densities of TEC variation (unfiltered data) observed at the GPS stations before (Fig. 5a) and after (Fig. 5b) the volcanic eruption. It is clear that there are no spectral peaks for the GPS-TEC data before the eruption (Fig. 5a). The spectral peaks at rgao, cauq and nihu after the eruption are at (176, 209, 260), (205, 172) and (203, 173, 252) s, respectively (Fig. 5b). Note that these periods of spectral peak after the eruption are shorter than those of the geomagnetic D component (major peak at 258 s). We discuss this point in the next section.

#### Discussion

As mentioned in “Introduction” section, Iyemori et al. (2015) confirmed that the MRs having period around 10–30 s observed almost all the time along the satellite

orbit by Swarm satellites are the spatial structures of small-scale FACs, and they also suggested that the typical timescale of the magnetic fluctuations is about 200, 296 and 340 s for the meridional component and 340 s for the zonal component. Nakanishi et al. (2014) suggested that the small-scale FACs observed by CHAMP are caused by the ionospheric E-layer dynamo having the lower atmospheric origin. That is the reason why we trace the MRs observed by Swarm to the E-layer altitude along the geomagnetic field. By the tracing, we see the enhancement of the amplitude in the latitudes around the volcano and their conjugate points about 2 h after the eruption as shown in Fig. 3a–c, and this fact, including the latitudinal extent as discussed in Fig. 4, supports the above idea on the FAC generation in the E-layer.

As summarized in “[Satellite observation](#)” section, peak-to-peak amplitude of  $\delta B_y$  in Fig. 3b, which corresponds to zonal component of magnetic perturbations, is largest. This is consistent with Figure 8c in Zettergren and Snively (2015) and Figure 14 in Nakanishi et al. (2014). The difference of the amplitude between  $\delta B_y$  in our Fig. 3b and Figure 8c in Zettergren and Snively (2015) may come from the difference in LT (the observed LT and simulated LT are 18 and 12 h, respectively) and that in magnetic latitude (the magnetic latitude of the Calbuco volcano is 31.46°S). In particular, the effect of LT difference may be more significant. The magnetic conjugacy of the packet structures of the MRs is clearly seen in the dynamic spectra (Fig. 3e–g).

As mentioned in “[Satellite observation](#)” section, we can estimate the spatial scale of the wave packets in MRs above the volcano and its conjugate point. However, we have no clue to check the period of the gravity waves from lower atmosphere which generate the small-scale FACs.

As shown in Fig. 2 in this paper and Nakanishi et al. (2014), magnetic fluctuations along low-altitude satellite orbit are commonly observed in middle and low latitudes, but it may be reasonable to consider that the MRs in Fig. 3 are associated with the volcanic eruption, because the wave-packet structure of the MRs is roughly symmetric in the latitudinal direction from the volcano and from its conjugate point.

Note that the packet structure of H component of the geomagnetic fluctuations, as seen in the plot of 215–235 s band-pass-filtered data (see inside of a red rectangle in Fig. 4d), is similar to that of the TEC oscillations observed at nihu and cauq (Fig. 4b, c). This similarity strengthens the idea that the magnetic effect of the volcanic eruption was observed by both SW-B and ground magnetometer at Huancayo.

Sharp spectral peaks at 258 and 214 s in geomagnetic D component are shown in Fig. 5b. Note that the 4-min geomagnetic fluctuation just after the 2010 Chile

earthquake was only seen in D components (Iyemori et al. 2013) probably because it occurred in midnight when the ionospheric conductivity, in particular the Cowling conductivity, was low. These spectral peaks are close to the theoretical periods of the VAR between the ionosphere and the ground, i.e., 260–280, 220–230 and around 200 s. The relatively large amplitude variations before the eruption (Fig. 4d, e) may come from other sources, and they are enhanced because of still high Cowling conductivity before the sunset.

We interpret these observations as follows: The ionospheric plasma moves up and down in the E-layer due to the VAR induced by the volcanic eruption (the schematic diagram in Fig. 1), and both the TEC variation and the FACs generated through the E-layer dynamo were caused by the plasma motion. A magnetic effect of the FACs was observed at the SW-B and in the D component of the ground geomagnetic field.

The spectral peaks in Fig. 5b, 203 s at nihu, 205 s at cauq, 209 s at rgao, roughly correspond to the theoretical periods of second overtone ( $\sim 200$  s) of the VAR between the ionosphere and the ground (Nishida et al. 2000). On the other hand, the major spectral peak of the geomagnetic field in Fig. 5b is close to the period of fundamental mode (260–270 s). These results strongly support the idea that the VAR induced by the volcanic eruption causes the disturbances of electron density in the F-region of the ionosphere as well as the geomagnetic variation on the ground. We consider that relatively short-period (200–210 s) AGWs, which could reach the ionospheric F-layer through the cutoff region for longer-period acoustic waves of fundamental mode, generate the TEC variations. On the other hand, the geomagnetic fluctuations observed at Huancayo resulting from long-period (250–260 s) AGWs which reach the ionospheric E-layer but couldn't reach F-region, generate the dynamo currents and cause the FACs. The TEC data derived from a GPS satellite PRN03 seen at cauq and nihu indicate the horizontal propagation of the TEC wave clearly, and the velocity is estimated to be about 720 m/s from the difference in the onset time of the 4-min TEC oscillations and the distance between the volcano and the sub-ionospheric point (SIP), where the GPS satellite-ground station links intersect the ionospheric shell at 300 km altitude, for each GPS station. The horizontal wave length, about 160 km derived from 720 m/s  $\times$  200 s (major spectral peak at nihu after the eruption), is comparable with the scale estimated for the FAC observed by the SW-B (about 180 km) and also with the results of the simulation (see Zettergren and Snively 2015, Figure 4c, f). The longer the distance between the volcano and the SIP is, the smaller the amplitude of the 4-min TEC oscillations becomes.

The distance, where the amplitude is zero, is estimated to be about 800 km from their attenuation rate if we assume that the amplitude is linearly attenuated. Therefore, a spatial extent of the ionospheric disturbance is estimated to be about 1600 km if TEC waves propagate concentrically, and the scale (1600 km) roughly corresponds to the latitudinal scale of MRs observed by the SW-B (1700 km).

As for the 608-s time difference between the packet structure in Fig. 4c, d, it could be interpreted as the effect of instantaneous propagation of the east–west dynamo electric field induced by the VAR above the volcano to the magnetic equator. This instantaneous propagation mechanism was proposed by Kikuchi and Araki (1979), and Araki (1994) applied it to the preliminary reverse impulse (PRI) of sudden impulse (SI). Although the horizontal scale is much shorter than that of PRI, the east–west ionospheric current caused by the instantaneously propagated electric field and the high Cowling conductivity on magnetic equator generates the geomagnetic fluctuations in the H component on the ground. On the other hand, the TEC wave propagated from the volcano to the GPS station, nihu with velocity of 720 m/s, i.e., near the acoustic velocity. The distance between the volcano and the GPS station is 574.96 km at the altitude of 300 km, which is close to 470 km distance derived from  $720 \text{ m/s} \times 608 \text{ s}$ .

Based on the above consideration, we suggest that both the spectral peaks of the magnetic field observed at Huancayo and the 4-min TEC oscillations around the volcano after the eruption are originated from the AGWs induced by the volcanic eruption, and the origin of the amplitude enhancements of MRs above the volcano and its conjugate point are also the same.

### Summary and conclusion

In this study, we investigated MRs observed by the SWARM satellite, geomagnetic fluctuations at Huancayo, and TEC variations in the ionosphere after the 2015 eruption of Chile's Calbuco volcano. The main results are summarized as follows.

1. The amplitudes of small-scale MRs observed by SW-B are enhanced above the volcano and over its geomagnetic conjugate point, and the enhanced regions have packet-like structure. An assumption that the AGWs caused by the eruption resulted in the small-scale FACs gives a consistent explanation for the MRs. The latitudinal extension of the wave packet, i.e., the scale of ionospheric E-layer dynamo region is about 1700 km, and the dominant wave length is about 180 km.
2. Geomagnetic field variation in D component with sharp spectral peaks after the eruption having the periods near the fundamental mode of vertical acoustic resonance is observed at Huancayo Geomagnetic Observatory, located at the same longitude as the volcano and on the magnetic equator.
3. The dominant periods of the TEC variation, i.e., about 200 s, after the eruption are also close to the theoretically predicted periods of the second overtone of VAR between the ionosphere and the Earth's ground. The horizontal propagation velocity, spatial scale and horizontal wave length of the 4-min TEC oscillations are estimated to be about 720 m/s, 1600 and 160 km, respectively.

These results are roughly consistent with consequences of simulations in Zettergren and Snively (2015) and support the idea that the atmospheric disturbances which cause the small-scale FACs in middle and low latitudes, i.e., MRs, are the acoustic mode waves.

In this paper, we analyzed only one event of volcanic eruptions, but the results add an example which supports the idea that the MRs in middle and low latitudes observed almost all the time by CHAMP or Swarm satellites can be caused by the AGWs propagated from the lower atmosphere. We still need more events observed by satellites for clarification of the MR source.

### Abbreviations

TEC: total electron content; MR: magnetic ripple; FAC: field-aligned current; VAR: vertical acoustic resonance; AGW: acoustic gravity wave; GPS: global positioning system; PSD: power spectral density; SIP: sub-ionospheric point.

### Authors' contributions

TA analyzed the data of the SWARM satellites and the total electron content and drafted the manuscript. TI analyzed the data of the ground geomagnetic field and helped to draft the manuscript. KN participated in the design of the study. MN provided the TEC data and performed initial analysis. DR, OV and ES observed the geomagnetic field at Huancayo and provided the data. All authors read and approved the final manuscript.

### Author details

<sup>1</sup> Graduate School of Science, Kyoto University, Kyoto, Japan. <sup>2</sup> National Institute of Information and Communications Technology, Tokyo, Japan. <sup>3</sup> Huancayo Geomagnetic Observatory Instituto Geofísico del Perú, Huancayo, Peru.

### Acknowledgements

This study is a part of the research proposal (ID: 10230) to the Swarm Science and Validation Opportunity Project under the ESA. The ground magnetic data at Huancayo and the TEC data are provided by Huancayo Geomagnetic Observatory, Instituto Geofísico del Perú and National Institute of Information and Communications Technology. This study was partially supported by JSPS KAKENHI Grant Number 15H05815 and 25287128 under Japan Society for Promotion of Science (JSPS).

Received: 17 February 2016 Accepted: 11 August 2016

Published online: 31 August 2016



## References

- Araki T (1994) A physical model of geomagnetic sudden commencement. *Geophys Monogr* 81:183–200
- Dautermann T, Calais E, Mattioli GS (2009) Global positioning system detection and energy estimation of the ionospheric wave caused by the 13 July 2003 explosion of the Soufrière Hills Volcano, Montserrat. *J Geophys Res* 114:B02202. doi:10.1029/2008JB005722
- Heki K (2006) Explosion energy of the 2004 eruption of the Asama Volcano, central Japan, inferred from ionospheric disturbances. *Geophys Res Lett* 33:L14303. doi:10.1029/2006GL026249
- Iyemori T, Nose M, Han D et al (2005) Geomagnetic pulsations caused by the Sumatra earthquake on December 26, 2004. *Geophys Res Lett* 32:1–4. doi:10.1029/2005GL024083
- Iyemori T, Tanaka Y, Odagi Y et al (2013) Barometric and magnetic observations of vertical acoustic resonance and resultant generation of field-aligned current associated with earthquakes. *Earth Planets Space*. doi:10.5047/eps.2013.02.002
- Iyemori T, Nakanishi K, Aoyama T et al (2015) Confirmation of existence of the small-scale field-aligned currents in middle and low latitudes and an estimate of time scale of their temporal variation. *Geophys Res Lett* 42:22–28. doi:10.1002/2014GL062555
- Kanamori H, Mori J (1992) Harmonic excitation of mantle Rayleigh waves by the 1991 eruption of Mount Pinatubo, Philippines. *Geophys Res Lett* 19(7):721–724
- Kikuchi T, Araki T (1979) Horizontal transmission of the polar electric field to the equator. *J Atmos Terr Phys* 41:927–936. doi:10.1016/0021-9169(79)90094-1
- Matsumura M, Saito A, Iyemori T et al (2011) Numerical simulations of atmospheric waves excited by the 2011 off the Pacific coast of Tohoku Earthquake. *Earth Planets Space* 63:885–889. doi:10.5047/eps.2011.07.015
- Nakanishi K, Iyemori T, Taira K, Lühr H (2014) Global and frequent appearance of small spatial scale field-aligned currents possibly driven by the lower atmospheric phenomena as observed by the CHAMP satellite in middle and low latitudes. *Earth Planets Space* 66:40. doi:10.1186/1880-5981-66-40
- Nishida K, Kobayashi N, Fukao Y (2000) Resonant oscillations between the solid earth and the atmosphere. *Science* 287:2244–2246
- Nishioka M, Tsugawa T, Kubota M, Ishii M (2013) Concentric waves and short-period oscillations observed in the ionosphere after the 2013 Moore EF5 tornado. *Geophys Res Lett* 40:5581–5586. doi:10.1002/2013GL057963
- Otsuka Y, Kotake N, Tsugawa T et al (2006) GPS detection of total electron content variations over Indonesia and Thailand following the 26 December 2004 earthquake. *Earth Planets Space* 58:159–165. doi:10.1186/BF03353373
- Park J, Lühr H, Stolle C et al (2009) The characteristics of field-aligned currents associated with equatorial plasma bubbles as observed by the CHAMP satellite. *Ann Geophys* 27:2685–2697. doi:10.5194/angeo-27-2685-2009
- Saito A, Tsugawa T, Otsuka Y et al (2011) Acoustic resonance and plasma depletion detected by GPS total electron content observation after the 2011 off the Pacific coast of Tohoku Earthquake. *Earth Planets Space* 63:863–867. doi:10.5047/eps.2011.06.034
- Sato K (1993) Small-scale wind disturbances observed by the MU radar during the passage of Typhoon Kelly. *J Atmos Sci* 50:518–537
- Shinagawa H, Iyemori T, Saito S, Maruyama T (2007) A numerical simulation of ionospheric and atmospheric variations associated with the Sumatra earthquake on December 26, 2004. *Earth Planets Space* 59:1015–1026
- Stolle C, Lühr H, Rother M, Balasis G (2006) Magnetic signatures of equatorial spread F as observed by the CHAMP satellite. *J Geophys Res* 111:A02304. doi:10.1029/2005JA011184
- Suzuki S, Vadas SL, Shiokawa K et al (2013) Typhoon-induced concentric air-glow structures in the mesopause region. *Geophys Res Lett* 40:5983–5987. doi:10.1002/2013GL058087
- Tahira M (1995) Acoustic resonance of the atmosphere at 3.7 Hz. *J Atmos Sci* 52:2670–2674
- Thébault E, Finlay CC, Beggan CD et al (2015) International geomagnetic reference field: the 12th generation. *Earth Planets Space* 67:79. doi:10.1186/s40623-015-0228-9
- Zettergren MD, Snively JB (2013) Ionospheric signatures of acoustic waves generated by transient tropospheric forcing. *Geophys Res Lett* 40:5345–5349. doi:10.1002/2013GL058018
- Zettergren MD, Snively JB (2015) Ionospheric response to infrasonic-acoustic waves generated by natural hazard events. *J Geophys Res A Space Phys* 120:8002–8024. doi:10.1002/2015JA021116

Submit your manuscript to a SpringerOpen® journal and benefit from:

- Convenient online submission
- Rigorous peer review
- Immediate publication on acceptance
- Open access: articles freely available online
- High visibility within the field
- Retaining the copyright to your article

Submit your next manuscript at ► [springeropen.com](http://springeropen.com)